Physics of the Earth and Planetary Interiors 276 (2018) 190–201

Contents lists available at ScienceDirect

Physics of the Earth and Planetary Interiors

journal homepage: www.elsevier.com/locate/pepi

On equatorially symmetric and antisymmetric geomagnetic secular variation timescales

Hagay Amit [a,*], Maélie Coutelier [a], Ulrich R. Christensen [b]

[a] CNRS, Université de Nantes, Nantes Atlantiques Universités, UMR CNRS 6112, Laboratoire de Planétologie et de Géodynamique, 2 rue de la Houssinière, F-44000 Nantes, France
[b] Max Planck Institute for Solar System Research, Justus-von-Liebig-Weg 3, 37077 Göttingen, Germany

ARTICLE INFO

Article history:
Received 1 December 2016
Received in revised form 28 April 2017
Accepted 28 April 2017
Available online 2 May 2017

Keywords:
Geomagnetic secular variation
Core flow
Core-mantle boundary
Equatorial symmetry

ABSTRACT

It has been suggested that the secular variation (SV) timescales of the geomagnetic field vary as $1/\ell$ (where ℓ is the spherical harmonic degree), except for the dipole. Here we propose that the same scaling law applies for SV timescales defined for different symmetry classes of the geomagnetic field and SV. We decompose the field and its SV into symmetric and antisymmetric parts and show in geomagnetic field models and numerical dynamo simulations that the corresponding SV timescales also vary as $1/\ell$, again except for the dipole. The time-average antisymmetric/symmetric SV timescales are larger/smaller than the total, respectively. The difference in SV timescales between these two symmetry classes is probably due to different degrees of alignment of the core flow with different magnetic field structures at the core-mantle boundary. The symmetric dipole SV timescale in the recent geomagnetic field and in long-term time-averages from numerical dynamos is below the extrapolated $1/\ell$ curve, whereas before ~1965 the geomagnetic dipole tilt was rather steady and the symmetric dipole SV timescale exceeded the extrapolated $1/\ell$ curve. We hypothesize that the period of nearly steady geomagnetic dipole tilt between 1810–1965 was anomalous for the geodynamo. Overall, the deviation of the dipole SV timescales from the $1/\ell$ curves may indicate that magnetic diffusion contributes to the dipole SV more than it does for higher degrees.

1. Introduction

Flow of an electrically-conducting fluid in Earth's outer core generates the geomagnetic field. The dynamics in the core leads to rapid temporal variations of the field termed the geomagnetic secular variation (SV). Measurements of the geomagnetic field and its SV allow to invert for the flow at the top of the core, but these flow models suffer from various types of inherent theoretical and numerical uncertainties (for a review see Holme, 2015). Alternatively, information on core dynamics may be gleaned directly from the power spectra of the field and its SV (Lowes, 1974). The SV timescales, based on the ratio between the power spectrum of the field and that of its SV, are interpreted as the times required for a given spherical harmonic component of the field to be reorganized, i.e. to become uncorrelated with its previous state (Hulot and LeMouël, 1994).

A scaling law for the SV timescales has been proposed and applied to geomagnetic field models and numerical dynamo models (Christensen and Tilgner, 2004; Lhuillier et al., 2011; Christensen et al., 2012; Bouligand et al., 2016). It has been shown that the SV timescales vary as $1/\ell$ (where ℓ is the spherical harmonic degree). Other (more complex) functions may also fit the observed SV timescales (Holme et al., 2011). However, the $1/\ell$ law is not only in agreement with observations and simulations but also theoretically expected assuming that magnetic diffusion is negligible in core dynamics on short timescales (Christensen et al., 2012).

The conventional field and SV power spectra are functions of ℓ, hence of the spatial scale alone, and do not distinguish between different symmetry properties of the field. Rotational effects are thought to be dominant in the core, suggesting an equatorial symmetry of the fluid flow (Taylor, 1917; Busse, 1970; Jault, 2008). This motivates us to study the SV timescales separately for their equatorially symmetric and antisymmetric parts. Consideration of the equatorially symmetric and antisymmetric field and/or SV (Roberts, 1971; Gubbins and Zhang, 1993) were previously invoked in various contexts, e.g. the geomagnetic dipole decrease (Amit and Olson, 2010), geomagnetic reversals (Coe and Glatzmaier, 2006), solar magnetic reversals (DeRosa et al., 2012) and planets' internal structure (Langlais et al., 2014). However,

* Corresponding author.
E-mail address: Hagay.Amit@univ-nantes.fr (H. Amit).

http://dx.doi.org/10.1016/j.pepi.2017.04.009
0031-9201/

such a decomposition has not yet been applied to the SV timescales.

The $1/\ell$ scaling law does not hold for the dipole, whose SV timescale is significantly underestimated by it. While the time-evolution of the dominantly antisymmetric (axial) dipole approximates the time-evolution of the dipole intensity (Gubbins, 1987; Olson and Amit, 2006; Finlay et al., 2016), the time-evolution of the symmetric (equatorial) dipole reflects the time-evolution of the dipole tilt (Amit and Olson, 2008). We will demonstrate that consideration of the symmetric and antisymmetric SV timescales may provide an insight into the behavior of the geomagnetic dipole tilt, in particular its long period of weak variability between 1810–1965.

Here we will show that the $1/\ell$ scaling law applies also for the SV timescales obtained for the equatorially symmetric and antisymmetric magnetic field and SV. A scaling law for the equatorially symmetric and antisymmetric SV timescales provides a more detailed glimpse into the behavior of the core field. It is not trivial that the total SV timescales which obey a $1/\ell$ dependence would partition in a way that their equatorially symmetric and antisymmetric parts would also obey the very same law (or any law at all). More specifically, even if the equatorially symmetric and antisymmetric parts do behave like τ_{sv}/ℓ, it is not obvious whether the same constant τ_{sv} applies for the total, symmetric and antisymmetric SV timescales.

The paper is organized as follows. In Section 2 we define the equatorially symmetric and antisymmetric SV timescales and their scaling laws. Statistical measures to evaluate the fits to the scaling laws are given in Section 3. In Section 4 we present the fits to geomagnetic field models and output from numerical dynamo simulations. We discuss our main findings in Section 5.

2. Theory

The power spectrum of the magnetic field at a radius r as a function of spherical harmonic degree ℓ is commonly defined (Lowes, 1974) as

$$R_\ell = (\ell+1)\left(\frac{a}{r}\right)^{(2\ell+4)}\sum_{m=0}^{\ell}[(g_\ell^m)^2 + (h_\ell^m)^2] \tag{1}$$

Similarly the power spectrum of the magnetic SV is

$$S_\ell = (\ell+1)\left(\frac{a}{r}\right)^{(2\ell+4)}\sum_{m=0}^{\ell}[(\dot{g}_\ell^m)^2 + (\dot{h}_\ell^m)^2] \tag{2}$$

In (1) and (2) g_ℓ^m and h_ℓ^m are the Gauss coefficients of the field for spherical harmonic degree ℓ and order m, $\dot{g}_\ell^m$ and $\dot{h}_\ell^m$ are the Gauss coefficients of the SV and a is Earth's radius. We use $a = 6371$ km for the surface of the Earth and $r = 3485$ km for the core radius.

The maps in Fig. 1 show the radial geomagnetic field and its symmetric and antisymmetric parts as well as the respective SV maps in 1980 based on the historical field model *gufm1* (Jackson et al., 2000). Note the stronger antisymmetric *Br* due to the contribution of the dominant axial dipole and the stronger symmetric SV. Fig. 1a shows that the geomagnetic field on the core-mantle boundary (CMB) is dominated by an axial dipole. Intense magnetic flux patches at high latitudes and reversed flux patches are pronounced deviations from axial dipolarity. In contrast, the SV is not dipole-dominated with large contributions by small scales (Fig. 1b). In addition, the SV is much more intense in the Atlantic hemisphere than in the Pacific (e.g. Bloxham et al., 1989; Gubbins et al., 2004; Holme et al., 2011) which may arise due to core-mantle thermal coupling (Christensen and Olson, 2003). The dipole dominance is evident in the geomagnetic power spectrum on the CMB. The rest of the spectrum is approximately white (Langlais et al., 2014). In contrast, the SV power is weakest for the dipole, and increases with ℓ.

Based on the power spectra R_ℓ and S_ℓ, the SV timescales are defined (Hulot and LeMouël, 1994) as

$$\tau_\ell = \sqrt{\frac{R_\ell}{S_\ell}} \tag{3}$$

These timescales are sometimes termed correlation times of the field, i.e. the time needed for the magnetic field at a given degree to become uncorrelated with its previous state. An analytic law was proposed to fit the SV timescale (Christensen and Tilgner, 2004; Lhuillier et al., 2011; Christensen et al., 2012; Bouligand et al., 2016):

$$\tau_\ell = \frac{\tau_{sv}}{\ell} \tag{4}$$

where τ_{sv} is a constant.

Most of the SV is thought to result from the advection and stretching of the magnetic field by the core flow. In general, an equatorially symmetric flow interacting with a symmetric/antisymmetric magnetic field would give a symmetric/antisymmetric local SV. Conversely, an antisymmetric flow interacting with a symmetric/antisymmetric magnetic field would give an antisymmetric/symmetric local SV. Analogous to (3) we define the symmetric and antisymmetric SV timescales as

$$\tau_\ell^s = \sqrt{\frac{R_\ell^s}{S_\ell^s}} \tag{5}$$

$$\tau_\ell^a = \sqrt{\frac{R_\ell^a}{S_\ell^a}} \tag{6}$$

where the superscripts s and a denote symmetric and antisymmetric parts, respectively. Similar to (4), we search for $1/\ell$ scaling laws for the symmetric and antisymmetric parts as well

$$\tau_\ell^s = \frac{\tau_{sv}^s}{\ell} \tag{7}$$

$$\tau_\ell^a = \frac{\tau_{sv}^a}{\ell} \tag{8}$$

where τ_{sv}^s and τ_{sv}^a are constants.

Finally, previous studies considered time-average spectra $\langle R_l\rangle$ and $\langle S_l\rangle$ to obtain a time-average SV timescale $\langle\tau_\ell\rangle$ (Lhuillier et al., 2011; Christensen et al., 2012; Bouligand et al., 2016):

$$\langle\tau_\ell\rangle = \sqrt{\frac{\langle R_\ell\rangle}{\langle S_\ell\rangle}} \tag{9}$$

In general, fits to $\langle\tau_\ell\rangle$ may be considered as more robust than fits to the instantaneous τ_ℓ at a given time.

3. Method

We decomposed the field and its SV to symmetric (even $\ell+m$) and antisymmetric (odd $\ell+m$) parts with respect to the equator. We then calculated their respective power spectra $R_\ell^s, R_\ell^a, S_\ell^s$ and S_ℓ^a. These spectra were used to calculate the symmetric and antisymmetric SV timescales τ_ℓ^s and τ_ℓ^a using (5) and (6) respectively.

We searched for linear fits in log–log scale to (4), (7) and (8). We concentrated on fits with a fixed exponent of -1 for the

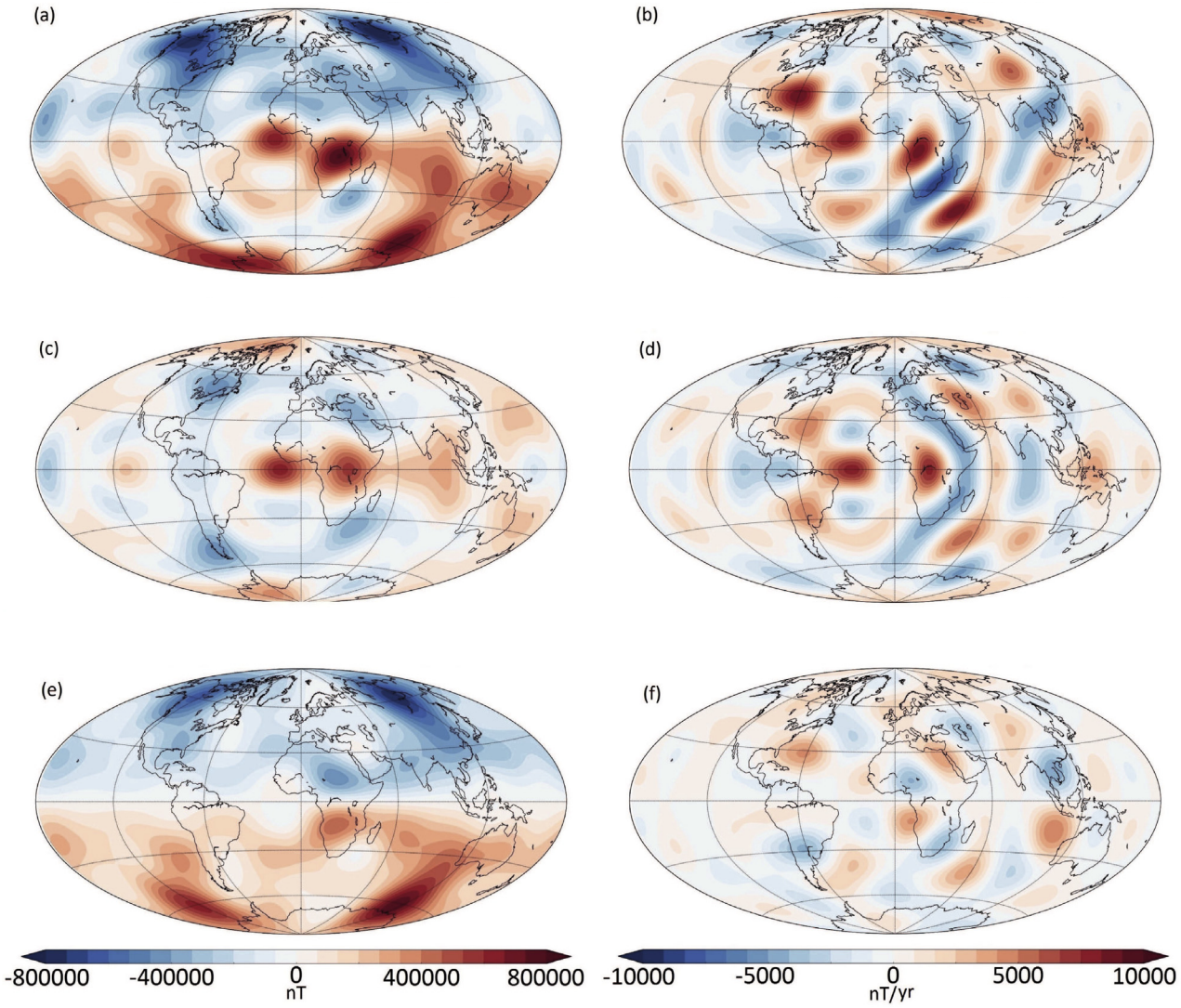

Fig. 1. Radial component of the geomagnetic field B_r (a, c, e) and its SV (b, d, f) on the CMB, including the total (a, b), symmetric (c, d) and antisymmetric (e, f) parts, based on the model *gufm1* (Jackson et al., 2000) in 1980.

ℓ-dependence, although we allowed in principle for arbitrary exponents γ. These fits were applied to the total (3), symmetric (5) and antisymmetric (6) SV timescales. Since it has been shown that the dipole, and in particular its dominant antisymmetric part, does not follow the same systematic behavior as higher multipoles do (Christensen and Tilgner, 2004; Lhuillier et al., 2011; Bouligand et al., 2016), we excluded the dipole from the fit. Following Lhuillier et al. (2011), the corresponding constants τ_{sv}, τ^s_{sv} and τ^a_{sv} were found using the F-distribution formalism. This is more appropriate than using a least squares fit, because even when the Gauss coefficients describing the field and its SV follow statistically a stationary Gaussian distribution with zero mean (Hulot and LeMouël, 1994), the ratios R_ℓ/S_ℓ are not distributed in a Gaussian way according to the Fisher-Snedkov distribution. According to this formalism the maximum likelihood of a power law $\tau_{sv}\ell^{-\gamma}$ is given by the maximum value of the following probability density function (pdf):

$$f(\tau_{sv},\gamma) = \prod_{\ell=2}^{\ell_{max}} F^{(2\ell+1)N_\ell,(2\ell+1)N_\ell}\left[\frac{(2\ell+1)N_\ell - 2}{(2\ell+1)N_\ell + 2}\left(\frac{\tau_\ell}{\tau_{sv}\ell^{-\gamma}}\right)^2\right] \qquad (10)$$

where $N_\ell = 1$ for a snapshot or an averaging time T shorter than $\langle 3\tau_\ell\rangle$ and $N_\ell = T/(3\langle\tau_\ell\rangle)$ for an averaging time longer than $\langle 3\tau_\ell\rangle$. Of particular interest are the pdf values for $\gamma = 1$. We simply denoted as F, F^s and F^a the maximum pdf values with $\gamma = 1$ for the total, symmetric and antisymmetric fits, respectively. For more details on the F-distribution see Appendix A of Bouligand et al. (2016).

4. Results

4.1. Geomagnetic field models

First we reproduced the results of previous studies for the $1/\ell$ dependence of the total geomagnetic SV timescales (Fig. 2) by fitting the analytic law (4). Fits were examined for different years. For the satellite field model CHAOS-4 (Olsen et al., 2014) only degrees until 13 were considered to avoid contamination by the crustal field. For the *gufm1* model (Jackson et al., 2000) in the period 1840–1990 the maximum degree was 10 as higher degrees might not be well resolved. Fig. 2a shows the F-distribution pdf

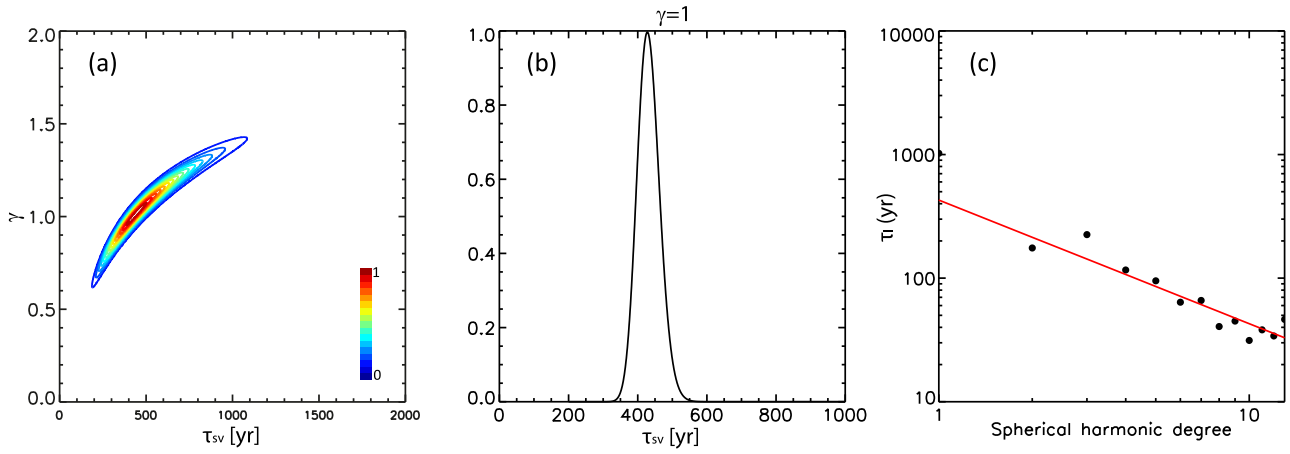

Fig. 2. Geomagnetic SV timescales τ_ℓ based on the model CHAOS-4 in 2005. (a) The normalized pdf of the F-distribution as a function of the prefactor τ_{sv} and the exponent γ; (b) Cross-section of (a) for $\gamma = 1$; (c) The resulting fit.

for a snapshot from CHAOS-4. The pdf takes the form of a crescent (Lhuillier et al., 2011; Bouligand et al., 2016). In this particular snapshot the cross-section of the pdf at exponent −1 (Fig. 2b) peaks practically at 1, i.e. the $1/\ell$ law is favored over any other exponent. Fig. 2c shows the resulting $1/\ell$ law fit to the total SV timescales. In Table 1 we report the best fit τ_{sv} values. We also report their 90% confidence intervals, i.e. the range into which 90% of the integral over the pdf falls. In the CHAOS-4 snapshot shown in Fig. 2, the 90% confidence interval amounts to ∼11–14% deviations from the best fit value of 428 years.

Fig. 3 shows the F-distribution results for the symmetric and antisymmetric SV timescales. Similar crescent shape pdf distributions as for the total SV timescales are found. For the CHAOS-4 model in 2005, the fits for τ^s_ℓ have a slightly lower F^s value than the fits for the total τ_ℓ, although the F^s value is still large hence the fit is significant. In contrast, the F^a value is very low (Table 1), with a significantly larger than one exponent ($\gamma \sim 1.3$) being favored (Fig. 3d). We will later show that this is not systematic; at other snapshots the F^a value may be very high whereas a low value may be found for F^s. In the CHAOS-4 model, the three best fitting SV timescales for $\gamma = 1$ τ_{sv}, τ^s_{sv} and τ^a_{sv} are found comparable, in the range ∼360–460 years (Figs. 2 and 3 and Table 1).

Table 1
The constant τ_{sv} in years calculated for the fits with different symmetries (*t* denotes total, *s* denotes symmetric and *a* denotes antisymmetric) and at different sampled times (2000–2010 from CHAOS-4 (Olsen et al., 2014) and 1840–1990 from *gufm1* (Jackson et al., 2000)). The last lines are the results for the time-average over the period 1840–1990 using $\langle R_l \rangle$ and $\langle S_l \rangle$. For each fit the maximum probability value is given in bold with the 90% confidence interval around it. The normalized pdf of the maximum probability for exponent −1 is *F*.

Year	Sym	τ_{sv}	*F*
2000	*t*	368 **414** 470	0.85
	s	373 **421** 480	1.00
	a	359 **404** 460	0.02
2005	*t*	381 **428** 486	1.00
	s	411 **463** 529	0.94
	a	346 **389** 443	0.11
2010	*t*	356 **400** 454	0.81
	s	392 **442** 505	0.98
	a	319 **359** 410	0.001
1900	*t*	434 **503** 596	0.49
	s	431 **502** 597	0.07
	a	441 **510** 602	0.59
1940	*t*	404 **468** 552	0.89
	s	363 **421** 498	0.79
	a	491 **569** 675	1.00
1980	*t*	422 **489** 579	0.90
	s	383 **445** 527	0.94
	a	519 **605** 723	0.10
⟨1840 − 1990⟩	*t*	422 **488** 576	0.86
	s	390 **452** 534	0.46
	a	475 **550** 649	0.86

The geomagnetic field is characterized by rapid dynamics with a magnetic advection time on the order of decades, demanding analysis over a longer timescale. Fig. 4 shows the three SV timescales as a function of spherical harmonic degree for three selected years from *gufm1*. For 1940 and 1980 τ^a_{sv} is the largest and τ^s_{sv} is the smallest of the three constants (Figs. 4b and c), while in 1900 the three constants are comparable (Fig. 4a). In 1940 and 1980 the difference between τ^a_{sv} and τ^s_{sv} reached ∼ 150–160 years. The corresponding four 90% confidence intervals span ∼140–200 years (Table 1). This means that accounting for uncertainties gives acceptable τ^a_{sv} and τ^s_{sv} values in 1940 and 1980, i.e. their difference is likely significant.

For different snapshots the optimum values of τ^s_{sv} or τ^a_{sv} may vary by up to 100 yr, i.e. in the same range as the possible systematic differences between τ^s_{sv} and τ^a_{sv}. The chaotic nature of the geodynamo seems to imply that fits to (4) for single snapshots may not be very representative. Averaging R^s_ℓ and S^s_ℓ (and likewise R^a_ℓ and S^a_ℓ) over a longer time span and using (9) will probably give a more robust result. In Fig. 6 we therefore examine the SV timescales obtained from the time-average geomagnetic field and SV spectra (Fig. 5) over the historical period 1840–1990 based on the model *gufm1* (Jackson et al., 2000). Fig. 6 shows less scatter and a better agreement compared to Fig. 4. Indeed the *F* and F^a values for the time-average SV timescales are large while F^s is moderate (Table 1). The pdf crescents are relatively narrow (Fig. 6a, d and g), the peak of the pdf for τ^s_{sv} lies well outside the 90% confidence interval for τ^a_{sv} and vice versa, and only a marginal overlap is found for the 90% confidence intervals of τ^a_{sv} and τ^s_{sv} (compare e.g. Fig. 6e and h).

Table 1 summarizes the SV timescales obtained for the geomagnetic field models. The historical field model results in overall somewhat longer τ_{sv} for *gufm1* compared to CHAOS-4, with differences of about ∼75, 10 and 165 years for the total, symmetric and antisymmetric fields, either because of the stronger temporal regularization in *gufm1* or simply due to natural fluctuations of the SV. For the time-average of the *gufm1* field and SV over the period 1840–1990, the antisymmetric SV timescale is 22% longer than the symmetric.

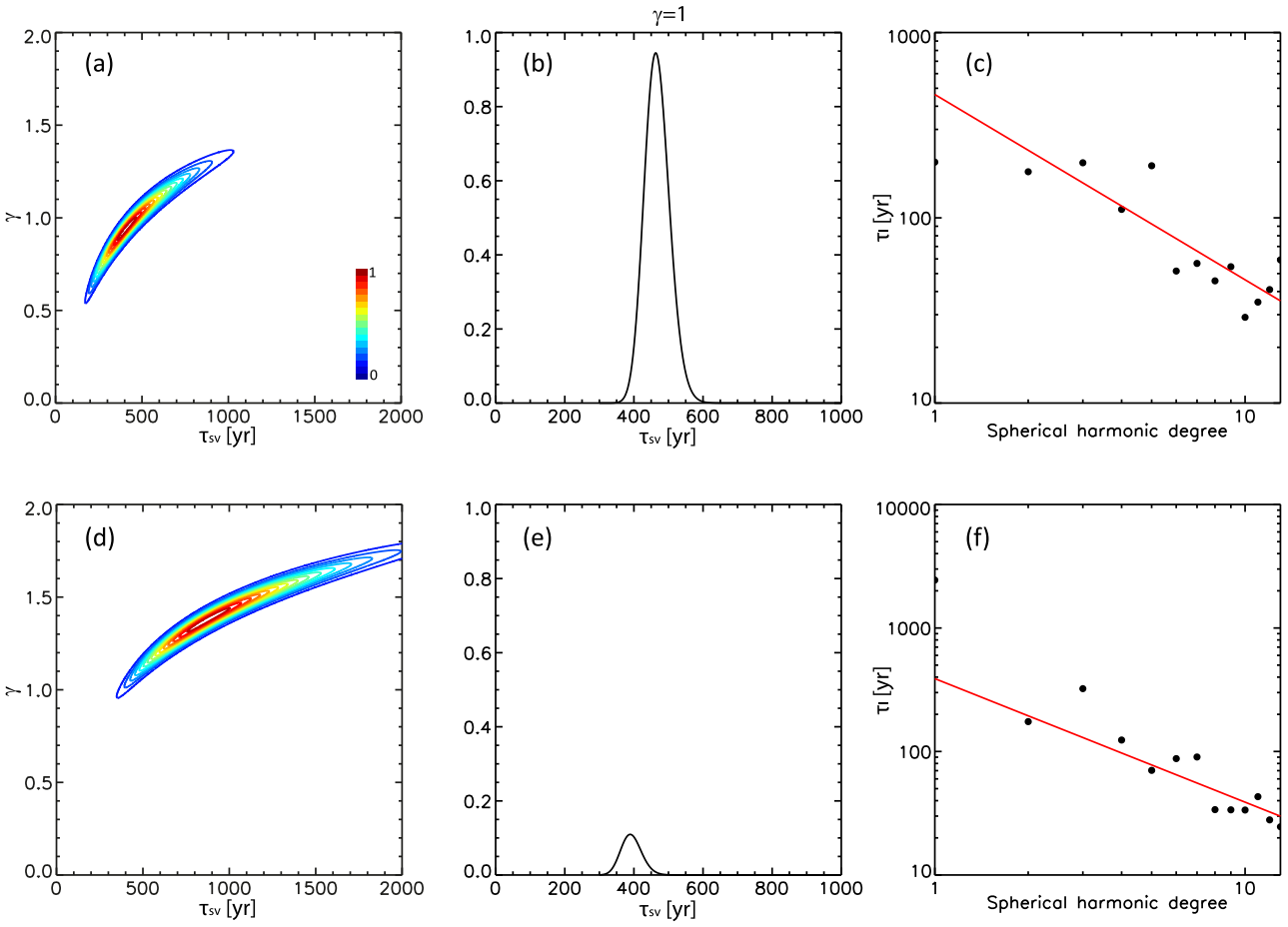

Fig. 3. As in Fig. 2 for the symmetric (a-c) and antisymmetric (d-f) SV timescales based on the model CHAOS-4 in 2005.

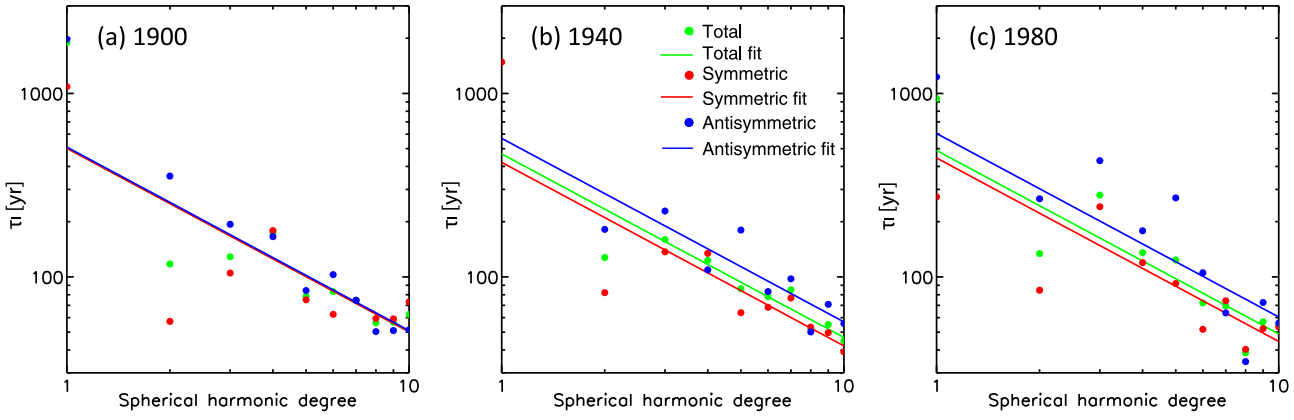

Fig. 4. Fits for the SV timescales based on the model *gufm1* for the years 1900 (a), 1940 (b), and 1980 (c). τ_ℓ, τ_ℓ^s and τ_ℓ^a are in green, red and blue, respectively. (For interpretation of the references to colour in this figure caption, the reader is referred to the web version of this article.)

Although the dipole is excluded from the fits, it is worth noting that the symmetric dipole is rather well fitted by the corresponding time-average curve (Fig. 6f). This is not the case for neither the recent field where the linear fits overestimate the symmetric dipole (Figs. 3c and 4c) nor for the early historical field where the fits underestimate τ_1^s (Fig. 4a and b). As shown in Fig. 7a, the reason for this behavior is related to a rather abrupt variability of the geomagnetic dipole tilt. Here we consider the *gufm1* model from 1590 because the Gauss dipole coefficients are probably well constrained even for the early period. Between 1810–1965 the tilt was nearly constant with an average absolute tilt change rate of 0.003°/year. However, between 1590 and 1810 the dipole axis drifted equatorward rapidly from 4.59° to 11.31° at an average rate of 0.030°/year, and between 1965–2010 the dipole axis drifted poleward rapidly (Amit and Olson, 2008) from 11.47° to 9.98° at an average rate of 0.033°/year, i.e. in the period 1810–1965 the dipole tilt rate of change was an order of magnitude slower than at the earlier and later periods. Consequently, between 1810–1965 S_1^s was very small, leading to an anomalously large τ_1^s in that period. In contrast, at other times during the past 420 years S_1^s was

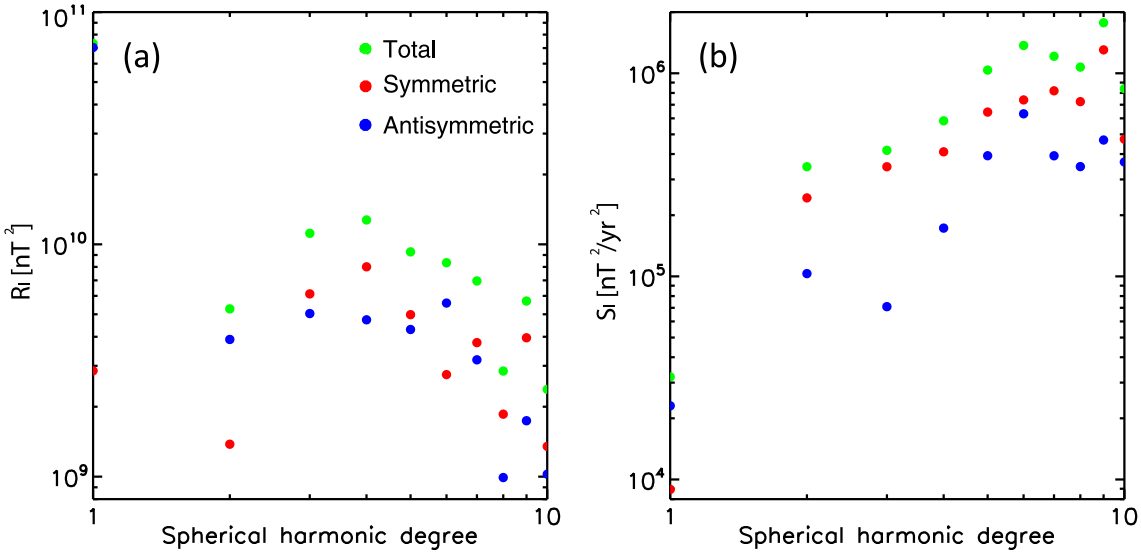

Fig. 5. Time-average geomagnetic field spectra $\langle R_l \rangle$ (left) and time-average SV spectra $\langle S_l \rangle$ (right) based on the model *gufm1* over the period 1840–1990. Total, symmetric and antisymmetric parts are in green, red and blue, respectively. (For interpretation of the references to colour in this figure caption, the reader is referred to the web version of this article.)

larger and the resulting τ_1^s was smaller. Aside from changes in the dipole tilt angle, azimuthal drift of the dipole axis also contributes to S_1^s. In fact, given the nearly constant tilt angle between 1810–1965, most of the power in S_1^s during this period must result from azimuthal drift of the dipole axis. However, the azimuthal drift has been exhibiting moderate temporal variability (Fig. 7b) about an average rate of 0.09 °/year. We will further elaborate on the anomalous nature of the steady geomagnetic tilt episode in light of the results from the analysis of numerical dynamos below.

4.2. Numerical dynamos

Next we examine the SV timescales in a set of numerical dynamo models from Christensen et al. (2012). The clear advantage here is the much longer averaging time compared to the historical period for which decent quality geomagnetic field data is available. The five dynamo models were analyzed over ∼20–120 advection times. Assuming a typical core flow velocity of $5 \cdot 10^{-4}$ m/s (e.g. Holme, 2015) and using the outer core thickness as a typical length scale, the advection time of the core is $\tau_u \sim 140$ yr. The 150 yr of the historical period therefore corresponds to about one advection time. The selected dynamo models (Table 2) span a range of control parameters, resulting in a range of magnetic Reynolds numbers (one order of magnitude differences). As for the geomagnetic field models, the fits are applied to the total τ_ℓ (3), symmetric τ_ℓ^s (5) and antisymmetric τ_ℓ^a (6) SV timescales. All SV timescales were calculated from the time-average field and SV spectra (9) using the same F-distribution formalism as was applied for the geomagnetic field, with the only difference being that $N_\ell = 1$ for the geomagnetic spectra whereas $N_\ell = T/(3\langle\tau_\ell\rangle)$ for the time-average spectra from the dynamo models (Lhuillier et al., 2011; Bouligand et al., 2016). The SV timescales are given in units of magnetic advection times in Table 2. Setting one advection time to 140 yrs results in $\langle\tau_{sv}\rangle$ values between ∼485 and 570 yrs for the different dynamo models, in decent agreement with the 488 years value for the time-average geomagnetic field (Table 1).

Fig. 8 shows the results for three models from Christensen et al. (2012). The dynamo models total magnetic power spectra R_ℓ are dominated by the dipole with an approximately flat spectra for the non-dipole terms, as in the geomagnetic field power spectra (Fig. 5a). In some dynamo models the antisymmetric field dominates (e.g. model 2 in Fig. 8a), in others the powers in the antisymmetric and symmetric fields are comparable (e.g. model 3 in Fig. 8d). In most dynamo models the powers in the antisymmetric and symmetric SV are generally similar except in model 5 which shows a slight dominance of the symmetric SV (Fig. 8h).

Table 2 summarizes the $1/\ell$ fits of the SV timescales for the dynamo models. When expressed in units of magnetic advection times, our five dynamo models span a fairly narrow range of values. For example, the total SV timescales of the five dynamo models cover a range of ∼3.5–4 magnetic advection times, despite an order of magnetic variability in the magnetic Reynolds number among the models. In contrast, Bouligand et al. (2016) found a larger variability of factor ∼2 in the total SV timescales among their dynamo models. The fits for the symmetric and antisymmetric SV timescales are rather decent in dynamo models 3–5 with significant F^s and F^a values. The F^a values are also significant in models 1–2, but in these models the F^s (as well as F) values are low. In all dynamo models the symmetric/antisymmetric SV timescales are smaller/larger than the total, respectively, except for model 4 where the three constants are practically identical. Also in model 3 the differences are relatively small, whereas in models 1, 2 and 5 $\langle\tau_{sv}^a\rangle$ is larger than $\langle\tau_{sv}^s\rangle$ by ∼20–35%. Our set of dynamo models is too small to identify a systematic dependence of the ratio $\langle\tau_{sv}^a\rangle/\langle\tau_{sv}^s\rangle$ on control parameters. However, we note that model 5 may be considered to be the most "Earth-like", as it has the lowest values for the Ekman and magnetic Prandtl numbers and at the same time a magnetic Reynolds number that is representative for the geodynamo. The differences between symmetric and antisymmetric SV timescales in the dynamo models are comparable to those in the geomagnetic field, where for the time-average period of 1840–1990 the antisymmetric SV timescale constant is 22% larger than the symmetric one, a difference that is very similar to that in our preferred model 5.

In the time-average SV timescales of the dynamo models the symmetric dipole is not well recovered by the $1/\ell$ law, whereas the symmetric quadrupole SV timescale is well fitted in most models (see e.g. model 3 in Fig. 8f). This is in contrast to the time-average geomagnetic SV timescales where the symmetric dipole SV timescale is adequately fitted but that for the quadrupole is not (Fig. 6f). Assuming that the time-average SV timescales in the

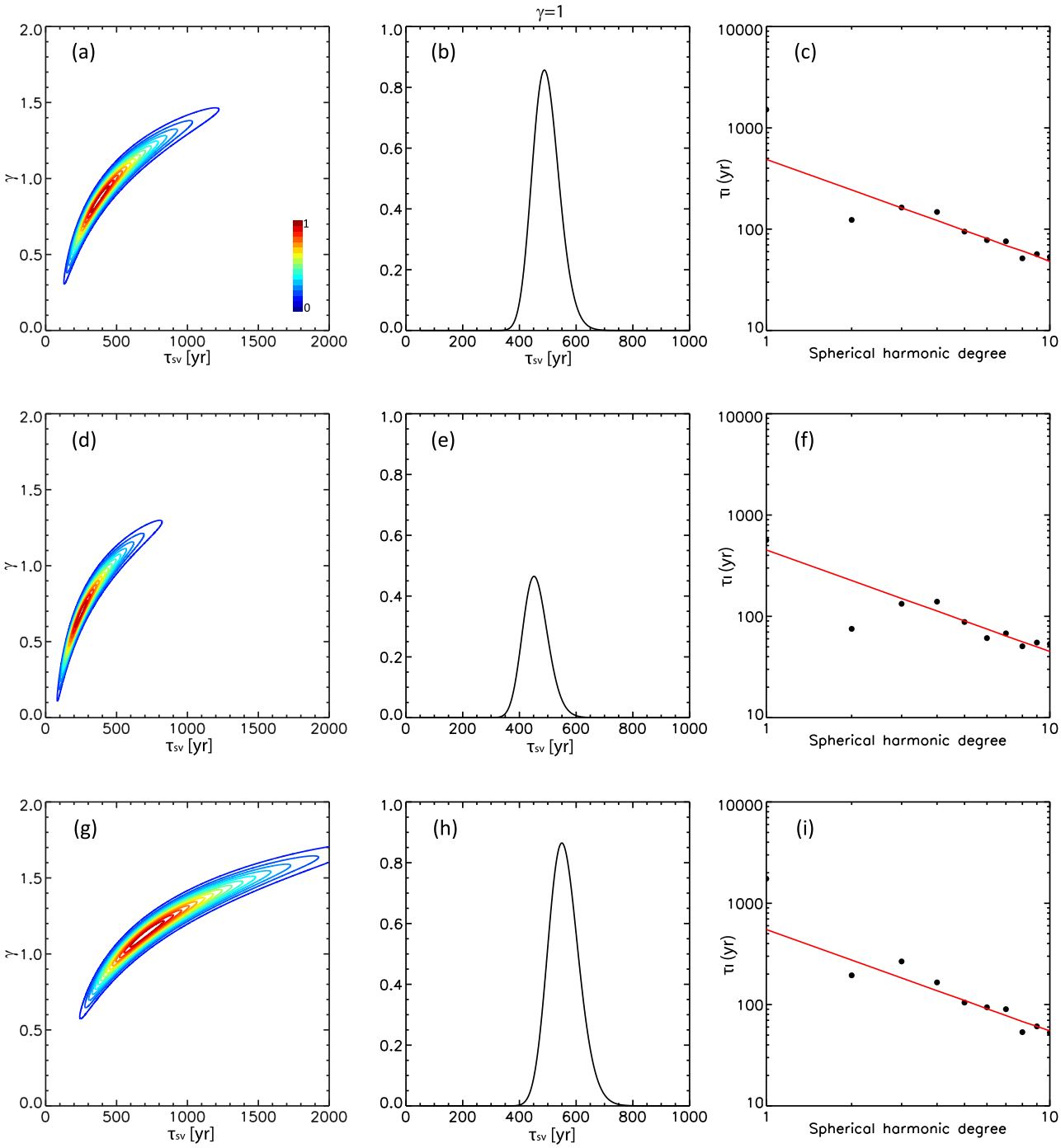

Fig. 6. Time-average geomagnetic SV timescales calculated from $\langle R_l \rangle$ and $\langle S_l \rangle$ based on the model *gufm1* over the period 1840–1990. The pdf of the F-distributions (a, d, g), the cross-sections for exponent −1 (b, e, h) and the resulting fitted SV timescales (c, f, i) are given for the total (a-c), symmetric (d-f) and antisymmetric (g-i) parts.

dynamo models are more representative of the true long-term mean than the geomagnetic SV timescales averaged over the historical period due to the much longer averaging time of the former, this may suggest that the SV timescale for the symmetric dipole is exceptionally large in the historical geomagnetic field and for the symmetric quadrupole it is exceptionally small (in both cases with respect to the symmetric SV timescales of higher degrees). This is demonstrated in Fig. 9 which shows the time-dependent magnetic dipole tilt in dynamo model 3 (middle row of Fig. 8d-f). During more than 60 magnetic advection times the tilt exhibited a typical oscillatory behavior of alternating rapid increase/decrease with rare quasi-steady periods (Fig. 9a). Assuming an advection time of 140 years, the average dipole tilt absolute rate of change of $\langle |\dot{\theta}_d| \rangle = 0.014°$/year in this dynamo model (Table 2) is about half the rate of change of the geomagnetic dipole tilt before 1810 or after 1965. In the other dynamo models $\langle |\dot{\theta}_d| \rangle$ varies in the range 0.007–0.021, on the same order though somewhat smaller than the geomagnetic values outside the quiet period, but significantly larger than the geomagnetic $\langle |\dot{\theta}_d| \rangle = 0.003°$/year value in the period 1810–1965.

In addition, the time fraction $T_{0.1}$ during which the dynamo models experienced an order of magnitude slower tilt changes than the average is rather small. For example, in the dynamo model

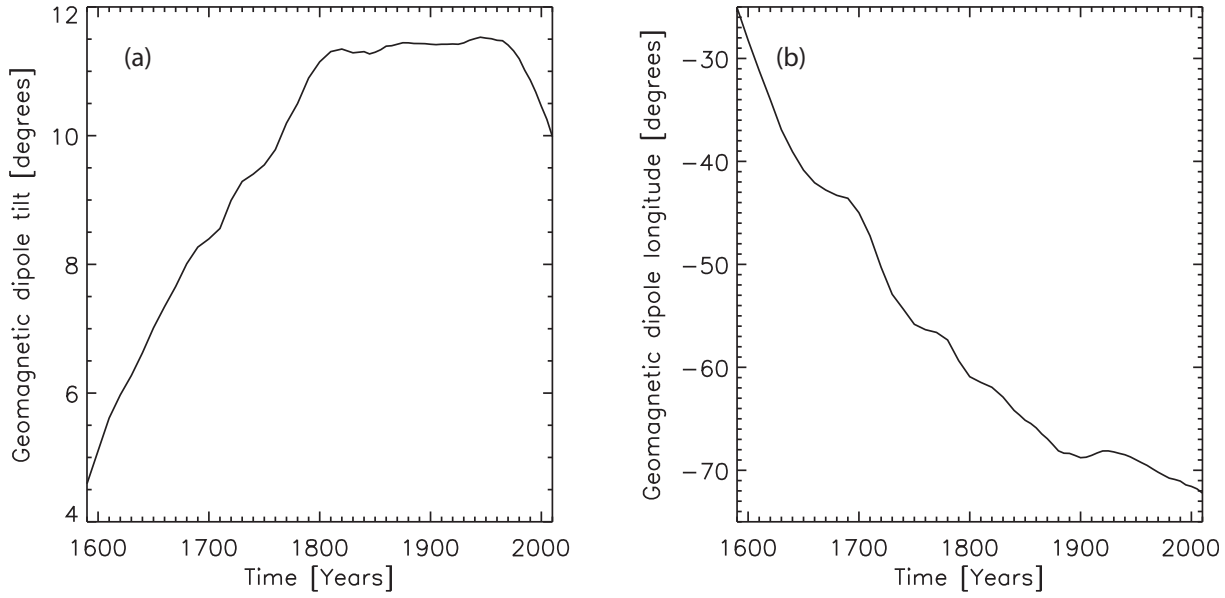

Fig. 7. Geomagnetic dipole tilt (a) and longitude (b), both in degrees, for the period 1590–2010. The dipole tilt is with respect to the geographic pole, the dipole longitude is with respect to the 0° meridional.

Table 2
Dynamo models. The control parameters are the Ekman number E, the Rayleigh number Ra and the magnetic Prandtl number Pm. The Prandtl number is $Pr = 1$ for all models. Also given the output magnetic Reynolds number Rm and the dipolarity f_{dip}. For parameters definitions and more details see Christensen et al. (2012). The time-average SV timescales constants are in units of magnetic advection times. The maximum pdf value for exponent −1 is given by F. The average absolute dipole tilt rate of change is given by $\langle|\dot{\theta}_d|\rangle$ in units of °/year. The relative time during which the absolute dipole tilt rate of change was smaller than 0.1 of its average value is given by $T_{0.1}$ in percentage.

Model	E	Ra	Pm	Rm	f_{dip}	Sym	$\langle\tau_{sv}\rangle$	F	$\langle\|\dot{\theta}_d\|\rangle$	$T_{0.1}$
1	10^{-4}	1.15×10^{8}	2	192	0.86	t	3.49 **3.60** 3.72	0.21	0.007	6%
						s	3.13 **3.22** 3.33	0.04		
						a	3.75 **3.89** 4.02	0.78		
2	10^{-4}	1×10^{9}	2	594	0.63	t	3.35 **3.46** 3.58	0.20	0.018	9%
						s	2.81 **2.90** 2.98	0.06		
						a	3.74 **3.87** 4.01	0.89		
3	3×10^{-5}	5×10^{9}	2.5	1030	0.58	t	3.92 **4.06** 4.19	0.79	0.014	8%
						s	3.83 **3.96** 4.08	0.57		
						a	3.96 **4.09** 4.24	1.00		
4	3×10^{-5}	5×10^{9}	5	1980	0.41	t	3.78 **4.02** 4.28	0.69	0.021	7%
						s	3.74 **3.97** 4.23	0.75		
						a	3.77 **4.01** 4.27	0.76		
5	10^{-5}	1×10^{11}	0.8	973	0.62	t	3.35 **3.51** 3.69	1.00	0.012	10%
						s	3.07 **3.22** 3.38	0.95		
						a	3.60 **3.79** 3.99	0.81		

shown in Fig. 9a $T_{0.1} = 8\%$ only, and similar low values of $T_{0.1} \sim 6$–10% are found for the other dynamo models (Table 2). To further illustrate this point we zoomed into three selected intervals of three advection times each (Fig. 9b, c and d), corresponding to the length of the historical period shown in Fig. 7. Clearly an event of quasi-steady tilt over a period of about one advection time as seen in the geomagnetic tilt between 1810–1965 (Fig. 7a) is rarely observed in the evolution of the dynamo model tilt (Fig. 9). In Fig. 9b a sustained rapid tilt increase event is seen, whereas in Fig. 9c the tilt decreases rapidly during most of the period. An event of slow tilt changes is observed in Fig. 9d during about one advection time. This holds for the other dynamo models, i.e. events of slow tilt changes do not last more than one advection time. In summary, as a rule the dynamo models exhibit rapid tilt changes comparable to the geomagnetic tilt changes prior to 1810 and after 1965. Episodes of slow tilt changes as observed between 1810–1965 are rare in the dynamo models.

5. Discussion

We find decent $1/\ell$ fits for the symmetric and antisymmetric SV timescales both in the geomagnetic field models and in the fields of several of our dynamo models when averaging in time. The symmetric/antisymmetric SV timescales are persistently smaller/larger than the total respectively. For the time-average geomagnetic field spectra we obtain a ratio of $\tau_\ell^s/\tau_\ell^a \sim 0.82$ (Table 1), while for the five analyzed numerical dynamo models this ratio ranges 0.75–0.99 (Table 2). Strong rotational effects in our dynamo models lead to flows that are dominated by an equatorially symmetric part. It has been argued that the same strong rotational effects are expected to prevail at Earth's core (e.g. Busse, 1970; Jault, 2008) and hence the flow at the top of the core is dominantly equatorially symmetric (Pais and Jault, 2008; Gillet et al., 2009, 2011, 2015). Core flow reconstructions based on statistics from numerical dynamos also exhibit a large level of equatorial symmetry (Aubert,

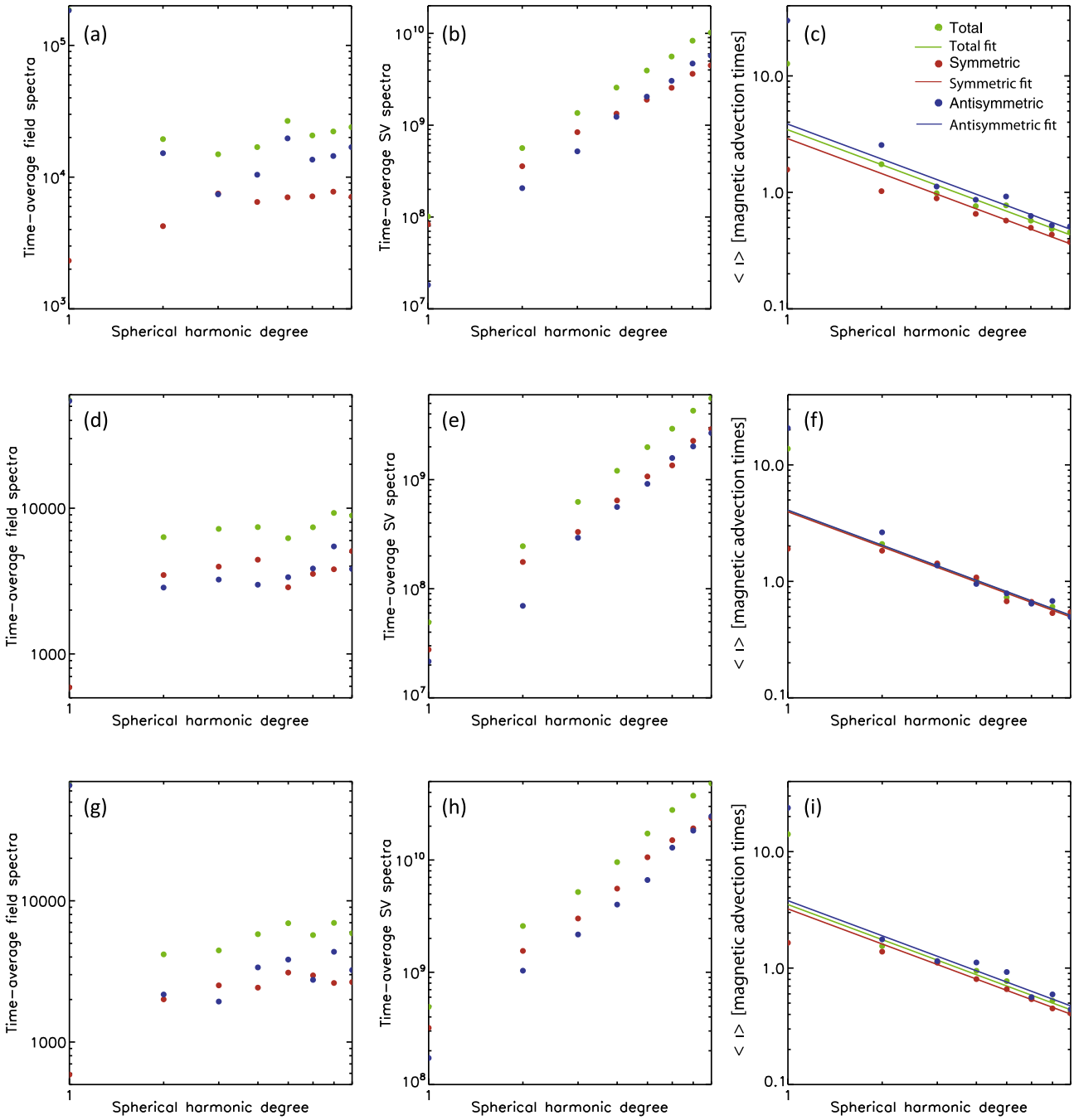

Fig. 8. Time-average spectra from dynamo models. Magnetic power spectra (a, d, g), SV power spectra (b, e, h) and SV timescales with the resulting fits for $\gamma = 1$ (c, f, i) for dynamo models 2 (top row), 3 (middle row) and 5 (bottom row). τ_ℓ, τ_ℓ^s and τ_ℓ^a are in green, red and blue, respectively. The field and SV power spectra are non-dimensional, the SV timescales are in units of magnetic advection times. (For interpretation of the references to colour in this figure caption, the reader is referred to the web version of this article.)

2013; Aubert et al., 2013; Finlay et al., 2016). However, some symmetry breaking may occur in a fully developed convective regime (Olson et al., 1999) or if boundary heterogeneity plays a major role (e.g. Amit et al., 2015). In Fig. 10 we show for dynamo model 5 the time-averaged velocity spectrum just below the Ekman layer near the outer boundary, separated into symmetric and antisymmetric parts. Up to degree 8 the power in the symmetric part is more than an order of magnitude larger than that in the antisymmetric part. At larger degrees, the difference shrinks and becomes less than a factor of two at degrees approximately larger than 20. We also note that 95% of the flow energy is in the toroidal component.

In the frozen flux approximation (Roberts and Scott, 1965), the change of the radial magnetic field near the CMB is given by

$$\frac{\partial B_r}{\partial t} = -\vec{u}_h \cdot \nabla_h B_r - B_r \nabla_h \cdot \vec{u}_h \tag{11}$$

where the suffix h refers to the tangential component. Obviously, a symmetric velocity field interacting with a symmetric magnetic field results in symmetric SV, and so does the interaction of an antisymmetric flow with an antisymmetric field. If the symmetries of the field and the flow are unlike, an antisymmetric SV results. Because the largest field component is the antisymmetric (axial)

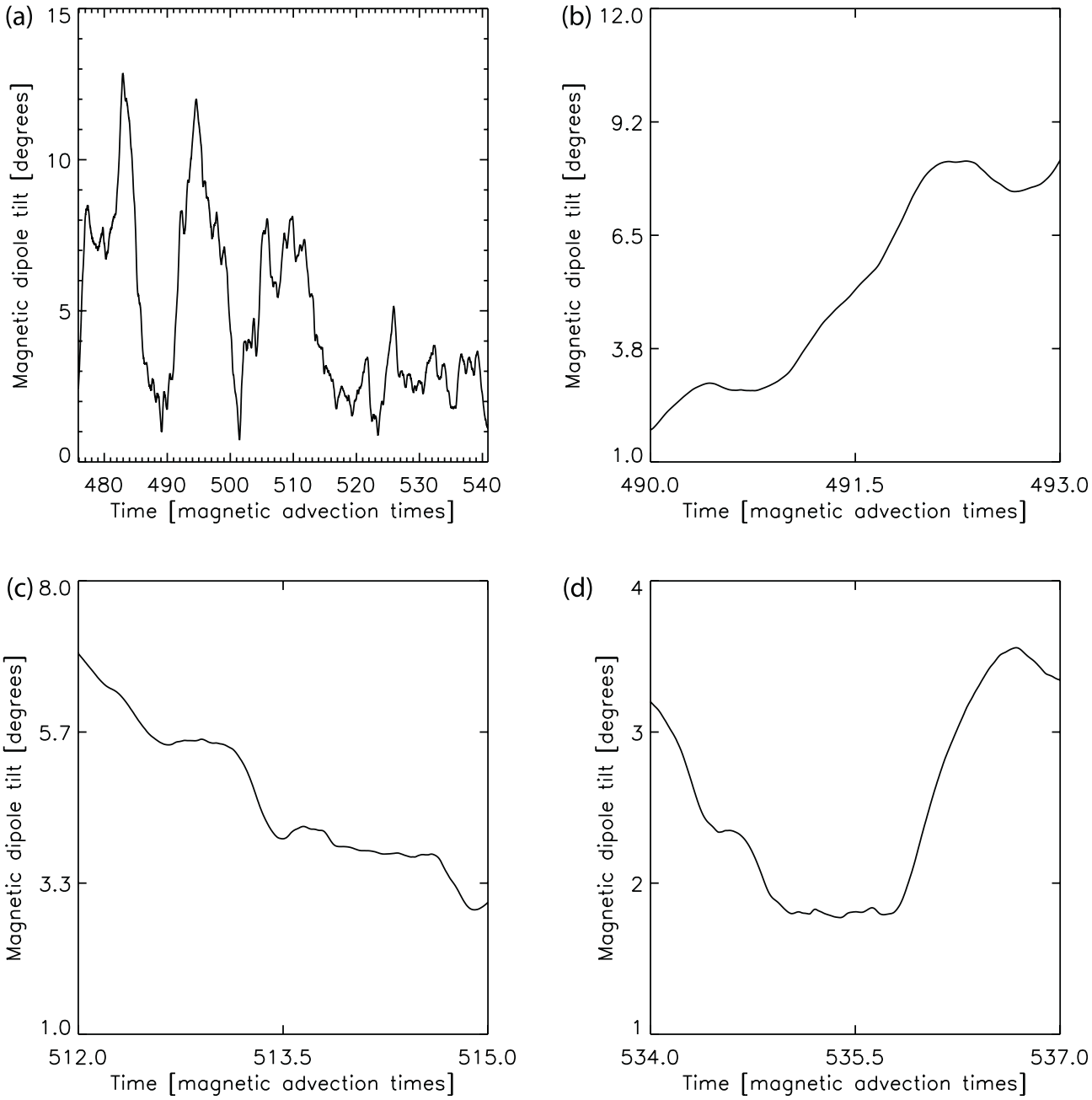

Fig. 9. Magnetic dipole tilt in dynamo model 3. The tilt is in degrees, time is in units of advection times. The tilt is shown for a long portion of the simulation (a) as well as during three intervals of three advection times each (b, c and d) which correspond to the duration of the historical period shown in Fig. 7. Note the tilt scale differences.

dipole and the flow is dominantly symmetric, one might naively assume that the SV must be dominantly antisymmetric. However, the symmetric and antisymmetric SV spectra are either comparable as in the dynamo models (Fig. 8) or the symmetric SV is larger as it is in the time-average geomagnetic field (Fig. 5b). Where is the signature of the dipole energy transfer? For a dominantly toroidal flow, for which $\nabla_h \cdot \vec{u}_h = 0$, the scale-dependence of the magnetic field rather than that of the flow matters for the SV according to (11). This scale is largest for the dipole, hence it makes a smaller contribution to SV than higher multipoles for a given field amplitude. In addition, to produce SV at a given degree, the dipole interacts only with a single toroidal flow component at exactly this degree (see selection rules; Bullard and Gellman, 1954; James, 1973), whereas several non-dipole field modes interact with several flow modes to contribute to the SV at any degree. Due to these reasons the contributions from the multipoles to the SV dominate over those from the axial dipole even though the latter contains the largest energy for a single degree. Indeed we found that in our dynamo models the SV fraction due to interactions of the flow with the dipole is merely 2–3% of the total SV.

The bias in the SV timescales in favor of larger values for the antisymmetric part may be caused by field-flow alignment and local advection efficiency. Flow along B_r contours on the CMB does not produce any SV. The ratio of symmetric/antisymmetric SV timescales would not reflect the ratio of symmetric/antisymmetric flows if one flow component is more aligned with the radial field and is therefore less efficient in producing SV. Finlay and Amit (2011) found that near high-latitude intense flux patches the flow is nearly field-aligned. These flux patches are prominent features of the antisymmetric magnetic field (compare Fig. 1a and e) and are

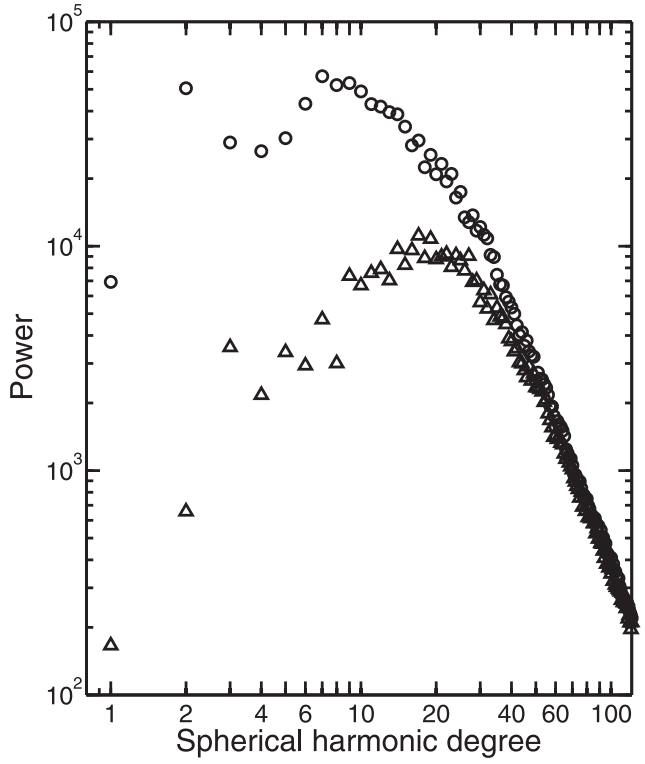

Fig. 10. Power spectra of the symmetric (circles) and antisymmetric (triangles) flow near the outer boundary of dynamo model 5.

associated with (symmetric) columnar flow in the dynamo models (Christensen et al., 1998) and presumably in the core (Gubbins and Bloxham, 1987). The strong antisymmetric SV that could be expected from this combination is largely diminished by the flow-field alignment. In contrast, Finlay and Amit (2011) found that drifting low-latitude patches (which have a strong equatorially symmetric component, compare Fig. 1a and c) are more characterized by flow perpendicular to B_r contours, leading to strong symmetric SV. For similar power in the symmetric and antisymmetric non-dipole field and a dominantly symmetric flow, these differences in the interaction of flow and field components leads to a preponderance of symmetric SV and therefore shorter symmetric than antisymmetric SV timescales.

The $1/\ell$ fit of the total SV timescales τ_ℓ is adequate for the non-dipole spectrum, but not for the dipole (Christensen and Tilgner, 2004; Lhuillier et al., 2011; Christensen et al., 2012; Bouligand et al., 2016). We found that the same holds for the symmetric τ_ℓ^s and antisymmetric SV timescales τ_ℓ^a where again only the non-dipole parts are well fitted by the $1/\ell$ law. Inferring SV timescales from the time-average spectra of *gufm1* shows that the fit of τ_ℓ^s recovers the symmetric dipole. However, this seems to be fortuitous since at earlier times τ_1^s is larger than the extrapolated $1/\ell$ fit (see e.g. Fig. 4a and b for 1900 and 1940) whereas at later times including at present-day as captured by the CHAOS-4 model τ_1^s is lower than the extrapolated $1/\ell$ fit (see Fig. 4c for 1980 and Fig. 3c for 2005). Results from the time-average spectra of the dynamo models indicate that the $1/\ell$ fit overestimates the symmetric dipole SV timescale, as in the present-day geomagnetic field. We therefore hypothesize that the nearly constant dipole tilt between 1810–1965 (Fig. 7a) was an anomalous event for the geodynamo. During this low tilt variability period the symmetric dipole SV power was exceptionally low, leading to an anomalously large symmetric dipole SV timescale.

Based on a formula of Moffatt (1978) for dipole moment vector changes, Amit and Olson (2008) developed an equation for the temporal change of the equatorial dipole. They combined core field and flow models to map advective sources and sinks of dipole tilt. Two major advective sinks that cause the recent tilt decrease were identified, one below Africa where positive flux is advected westward towards the negative equatorial pole, another below North America where negative flux is advected poleward away from the negative pole. Before 1965 these sinks were balanced by advective sources of dipole tilt at high-latitudes of the southern hemisphere, yielding little tilt change. The amplitude of the symmetric dipole SV timescale, which is directly related to whether the tilt varies rapidly or remains quasi-stationary, therefore depends on the subtle interaction between the flow and the field at the top of the core (Amit and Olson, 2008).

The axial (i.e. antisymmetric) dipole is special. Given the length of the historical geomagnetic field models, the stationary isotropic model of Hulot and LeMouël (1994) holds only for the non-axial dipole field. Moreover, Bouligand et al. (2016) showed that two timescales are needed to describe the variability of the axial dipole. In addition, and particularly concerning the equatorial dipole, it is possible that dipole SV timescales deviate from the $1/\ell$ law because the dipole SV violates the frozen-flux approximation more than higher degrees (Holme and Olsen, 2006). Strong zonal core flows (e.g. Hulot et al., 2002; Amit and Olson, 2006) do not produce SV of the axial dipole, hence dipole advection is possibly less efficient than the advection of higher degree terms that are less axial. Indeed, based on maps of advective sources and sinks of axial dipole change, advection accounts for only ~50–80% of the axial dipole change (Olson and Amit, 2006; Finlay et al., 2016). Explaining the dipole SV timescales (both axial and equatorial) as well as unraveling the role of magnetic diffusion in the SV remain challenges.

Our new fits for the symmetric and antisymmetric SV timescales provide more detailed insight into the re-organization times of particular spatial scales. Our results indicate that both the symmetric and antisymmetric SV timescales vary as $1/\ell$, as was previously found for the total. The symmetric part of the geomagnetic field gets re-organized relatively faster, whereas the antisymmetric part requires a longer time to become non-correlated with its previous state. Differences in the alignment between different magnetic field components with the local flow can plausibly be the cause for this difference. Ongoing measurements of the geomagnetic field by surface observatories and dedicated satellites like the current SWARM mission will shed more light on the geomagnetic SV timescales, which will provide more insight into the dynamics in Earth's core.

Acknowledgments

This study was supported by the Centre National d'Études Spatiales (CNES). We are grateful to two anonymous reviewers for constructive comments. H.A. thanks Claire Bouligand for insightful discussions.

References

Amit, H., Choblet, G., Olson, P., Monteux, J., Deschamps, F., Langlais, B., Tobie, G., 2015. Towards more realistic core-mantle boundary heat flux patterns: a source of diversity in planetary dynamos. Prog. Earth Planet. Sci. 2, 26. http://dx.doi.org/10.1186/s40645-015-0056-3.

Amit, H., Olson, P., 2006. Time-average and time-dependent parts of core flow. Phys. Earth Planet. Inter. 155, 120–139.

Amit, H., Olson, P., 2008. Geomagnetic dipole tilt changes induced by core flow. Phys. Earth Planet. Inter. 166, 226–238.

Amit, H., Olson, P., 2010. A dynamo cascade interpretation of the geomagnetic dipole decrease. Geophys. J. Int. 181, 1411–1427.

Aubert, J., 2013. Flow throughout the Earth's core inverted from geomagnetic observations and numerical dynamo models. Geophys. J. Int. 192, 537–556.
Aubert, J., Finlay, C.C., Fournier, F., 2013. Bottom-up control of geomagnetic secular variation by the Earth's inner core. Nature 502, 219–223.
Bloxham, J., Gubbins, D., Jackson, A., 1989. Geomagnetic secular variation. Phil. Trans. Roy. Soc. London A329, 415–502.
Bouligand, C., Gillet, N., Jault, D., Schaeffer, N., Fournier, A., Aubert, J., 2016. Frequency spectrum of the geomagnetic field harmonic coefficients from dynamo simulations. Geophys. J. Int. 207, 1142–1157.
Bullard, E.B., Gellman, H., 1954. Homogeneous dynamos and terrestrial magnetism. Phil. Trans. R. Soc. Lond. A 247, 213–278.
Busse, F., 1970. Thermal instabilities in rapidly rotating systems. J. Fluid Mech. 44, 441–460.
Christensen, U., Olson, P., 2003. Secular variation in numerical geodynamo models with lateral variations of boundary heat flow. Phys. Earth Planet. Inter. 138, 39–54.
Christensen, U., Olson, P., Glatzmaier, G., 1998. A dynamo model interpretation of geomagnetic field structures. Geophys. Res. Lett. 25, 1565–1568.
Christensen, U., Tilgner, A., 2004. Power requirement of the geodynamo from ohmic losses in numerical and laboratory dynamos. Nature 439, 169–171.
Christensen, U., Wardinsky, I., Lesur, V., 2012. Timescales of geomagnetic secular acceleration in satellite field models and geodynamo models. Geophys. J. Int. 190, 243–254.
Coe, R., Glatzmaier, G., 2006. Symmetry and stability of the geomagnetic field. Geophys. Res. Lett. 33, L21311. http://dx.doi.org/10.1029/2006GL027903.
DeRosa, M., Brun, A., Hoeksema, J., 2012. Solar magnetic field reversals and the role of dynamo families. Astrophys. J. 757, 96.
Finlay, C.C., Amit, H., 2011. On flow magnitude and field-flow alignment at Earth's core surface. Geophys. J. Int. 186, 175–192.
Finlay, C.C., Aubert, J., Gillet, N., 2016. Gyre-driven decay of Earth's magnetic dipole. Nature Commun. 7, 10422.
Gillet, N., Jault, D., Finlay, C.C., 2015. Planetary gyre, time-dependent eddies, torsional waves and equatorial jets at the Earth's core surface. J. Geophys. Res. 120, 3991–4013.
Gillet, N., Pais, M.A., Jault, D., 2009. Ensemble inversion of time-dependent core flow models. Geochem. Geophys. Geosyst. 10, Q06004.
Gillet, N., Schaeffer, N., Jault, D., 2011. Rationale and geophysical evidence for quasi-geostrophic dynamics within the Earth's core. Phys. Earth Planet. Inter. 187, 380–390.
Gubbins, D., 1987. Mechanism for geomagnetic polarity reversals. Nature 326, 167–169.
Gubbins, D., Bloxham, J., 1987. Morphology of the geomagnetic field and implications for the geodynamo. Nature 325, 509–511.
Gubbins, D., Gibbons, S., 2004. Low Pacific secular variation. In: Channell, J., Kent, D., Lowrie, W., Meert, J. (Eds.), Timescales of the Paleomagnetic Field, vol. 145. Geophysical Monograph, Washington D.C.
Gubbins, D., Zhang, K., 1993. Symmetry properties of the dynamo equations for paleomagnetism and geomagnetism. Phys. Earth Planet. Inter. 75, 225–241.
Holme, R., 2015. Large-scale flow in the core. In: Olson, P. (Ed.), Treatise on Geophysics. . second ed., vol. 8 Elsevier Science.
Holme, R., Olsen, N., 2006. Core surface flow modelling from high-resolution secular variation. Geophys. J. Int. 166, 518–528.
Holme, R., Olsen, N., Bairstow, F.L., 2011. Mapping geomagnetic secular variation at the core-mantle boundary. Geophys. J. Int. 186, 521–528.
Hulot, G., Eymin, C., Langlais, B., Mandea, M., Olsen, N., 2002. Small-scale structure of the geodynamo inferred from ersted and Magsat satellite data. Nature 416, 620–623.
Hulot, G., LeMouël, J.-L., 1994. A statistical approach to the Earth's main magnetic field. Phys. Earth Planet. Inter. 82, 167–183.
Jackson, A., Jonkers, A., Walker, M., 2000. Four centuries of geomagnetic secular variation from historical records. Phil. Trans. R. Soc. Lond. A358, 957–990.
James, R.W., 1973. The Adams and Elsasser dynamo integrals. Phil. Trans. R. Soc. Lond. A 331, 469–478.
Jault, D., 2008. Axial invariance of rapidly varying diffusionless motions in the earth's core interior. Phys. Earth Planet. Inter. 166, 67–76.
Langlais, B., Amit, H., Larnier, H., Thébault, E., Mocquet, A., 2014. A new model for the (geo)magnetic power spectrum, with application to planetary dynamo radii. Earth Planet. Sci. Lett. 401, 347–358.
Lhuillier, F., Fournier, A., Hulot, G., Aubert, J., 2011. The geomagnetic secular variation timescale in observations and numerical dynamo models. Geophys. Res. Lett. 38, L09306. http://dx.doi.org/10.1029/2011GL047356.
Lowes, F., 1974. Spatial power spectrum of the main geomagnetic field. Geophys. J. R. Astr. Soc. 36, 717–730.
Moffatt, H., 1978. Magnetic Field Generation in Electrically Conducting Fluids. Cambridge University Press, Cambridge, U.K..
Olsen, N., Lühr, H., Finlay, C.C., Sabaka, T.J., Michaelis, I., Rauberg, J., Tffner-Clausen, L., 2014. The CHAOS-4 geomagnetic field model. Geophys. J. Int. 197, 815–827.
Olson, P., Amit, H., 2006. Changes in earth's dipole. Naturwissenschaften 93, 519–542.
Olson, P., Christensen, U., Glatzmaier, G., 1999. Numerical modeling of the geodynamo: mechanisms of field generation and equilibration. J. Geophys. Res. 104, 10383–10404.
Pais, M.A., Jault, D., 2008. Quasi-geostrophic flows responsible for the secular variation of the Earth's magnetic field. Geophys. J. Int. 173, 421–443.
Roberts, P., Scott, S., 1965. On analysis of the secular variation, 1, a hydromagnetic constraint: Theory. J. Geomagn. Geoelectr. 17, 137–151.
Roberts, P.H., 1971. Dynamo theory. In: Reid, W.H. (Ed.), Mathematical problems in the geophysical sciences. Am. Math. Soc.
Taylor, G., 1917. Motion of solids in fluids when the flow is not irrotational. Proc. R. Soc. Lond. A. 93, 92–113.